Dynamic Mechanical Analysis Test for Evaluating Loose Sands on a Wide Strain Range-Application to the InSight Mission on Mars

María Juliana Chaparro López, Juan-Pablo Castillo-Betancourt, Miguel Cabrera, Bernardo Caicedo, Pierre Delage, Philippe Lognonné, Bruce Banerdt

Dynamic Mechanical Analysis test for evaluating loose sands on a wide strain range. Application to the InSight mission on Mars.

Maria-Juliana Chaparro-Lopez[1], Juan-Pablo Castillo-Betancourt[2], Miguel Cabrera[3], Bernardo Caicedo[4], Pierre Delage[5], Philippe Lognonné[6], Bruce Banerdt[7].

Reference

Chaparro López, M. J., Castillo-Betancourt, J.-P., Cabrera, M., Caicedo, B., Delage, P., Lognonné, P., & Banerdt, B. (2023). Dynamic Mechanical Analysis Test for Evaluating Loose Sands on a Wide Strain Range—Application to the InSight Mission on Mars. Geotechnical Testing Journal, 46(6).
https://doi.org/10.1520/gtj20230381.
https://hal-enpc.archives-ouvertes.fr/hal-04431625

[1] Civil Environmental Engineering Department, Universidad de Los Andes, Bogota D.C, Bogotá D.C, 111711, Colombia; https://orcid.org/0009-0004-7086-6026. **Corresponding author: mj.chaparro@uniandes.edu.co**
[2] Civil Environmental Engineering Department, Universidad de Los Andes, Bogota D.C, Bogotá D.C, 111711, Colombia; https://orcid.org/0000-0003-3123-4654.
[3] Faculty of Civil Engineering and Geosciences, Delft University of Technology, Delft, The Netherlands, 2628 CD; https://orcid.org/0000-0002-9236-8130.
[4] Civil Environmental Engineering Department, Universidad de Los Andes, Bogota D.C, Bogotá D.C, 111711, Colombia; https://orcid.org/0000-0003-4344-0914.
[5] Laboratoire Navier – CERMES, École nationale des Ponts et chaussées, 77420, France; https://orcid.org/ 0000-0002-2101-5522.
[6] Université Paris-Cité, Institut de Physique du Globe de Paris, 75006, France; https://orcid.org/0000-0002-1014-920X.
[7] Jet Propulsion Laboratory, NASA – CalTech, 91125, USA; https://orcid.org/0000-0003-3125-1542

ABSTRACT

The dynamic properties of loose sands under low stresses are an unexplored topic in soil dynamics because these soil conditions are uncommon in most geotechnical structures on Earth. However, low densities and low-stress conditions prevail on other planets, like, for instance, the surface of Mars, for which particular attention is presently given through the InSight NASA mission. This work presents a new procedure for measuring the dynamic properties of loose sand under low stress by using the Dynamical Mechanical Analysis (DMA) tester, a technique commonly used in asphalt engineering but not in geotechnical engineering. Compared to traditional geotechnical methods (Resonant Column and Cyclic Triaxial Tests), DMA investigates a broader range of strains using a single apparatus. In this work, we assess the dynamical properties of loose fine sand $Dr \approx 0.2$, considered a possible Mars regolith analog, by varying the input strain from $\gamma=10^{-6}$ to $\gamma=10^{-2}$ while applying confining pressures from σ_3=3 kPa to σ_3=30 kPa. The results validate the proposed procedure, showing an increment of the shear modulus as the confining pressure increases. Furthermore, they highlight DMA's advantages for studying the dynamic properties of granular soils under low stress and strain.

Keywords

Dynamic properties, Dynamical Mechanical Analysis (DMA), Rheometer, Loose sand, Martian simulant, low confining pressure.

NOMENCLATURE

σ_v	Basal suction
σ_3	Confining pressure
ξ	Damping ratio
G	Dynamic Shear Modulus.
ρ	Grain density
G_{max}	Maximum dynamic shear modulus
D_{50}	Median particle size.
C_u	Uniformity coefficient
γ_r	Reference shear strain
D_r	Relative density
θ	Rotation reported by the rheometer.
τ	Shear stress
γ	Shear Strain
γ_e	Shear strain in the elastic threshold
σ	Standard deviation
ψ	Suction
T	Torque
e	Void ratio

Introduction

The study of the dynamic properties of Martian regolith gained interest due to NASA's InSight mission on Mars (Interior Exploration using Seismic Investigations, Geodesy, and Heat Transport). InSight is a geophysical mission that successfully installed for the first time on the surface of Mars, in an area called Elysium Planitia, a high sensitivity very large band seismometer called SEIS (Seismic Experiment for Interior Structure), together with a self-driving thermal probe called HP3 (Heat Flow and Physical Properties Package). Both instruments provided detailed geophysical and mechanical data of the near-surface terrain. Figure 1 presents a photo taken at the beginning of the mission by the Instrument Context Camera (ICC) of the InSight lander, showing that the landing site, called Homestead Hollow, is flat and characterized by a sandy deposit with little rock abundance as planned from orbiter data during the landing site selection (Golombek et al. 2020). Figure 1 also shows, in the center, the semi-spherical white Wind and Thermal Shield (WTS) covering the SEIS seismometer to protect it from Martian winds (under an average atmospheric pressure of 600 Pa) and temperature changes (between -20°C and -80°C). The selection of the Martian regolith simulants was based on orbital thermal inertia measurements, geological considerations, and some observations from former rover missions (Golombek et al. 2008), suggesting that the Mars surface in Elysium Planitia is made up of loose sub-rounded to rounded sand with an average diameter of around D_{50}=175 μm.

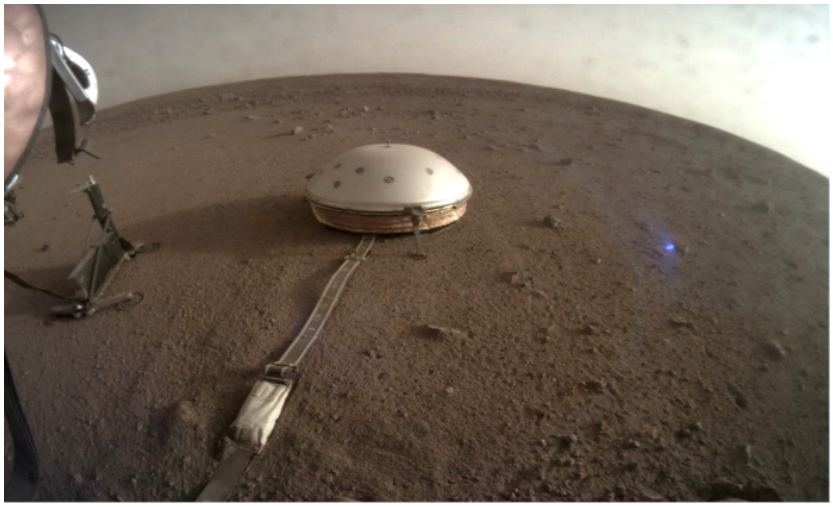

FIGURE 1. Instrument Context Camera view of the Wind and Thermal Shield (WTS) covering the SEIS seismometer in the centre and the HP^3 device on the left-hand side. The dome measures 60 cm in diameter. Image Credit: NASA-JPL. The foot consists of a disc with 60 mm diameter and a 20 mm long conic spike (10 mm diameter at its base) in its centre (Delage et al. 2022).

The physical properties of the surface regolith were further characterized by local thermal

measurements conducted with the HP^3 probe, which indicated a low thermal conductivity for the upper 3-37 cm of the soil (0.039 ± 0.002 W m^{-1} K^{-1}) from which quite a low density was derived, around 1.2 Mg/m^3 (Spohn et al. 2018). The very low-stress profile along the first 10 cm is related to the low gravity on Mars (3.73 m/s^2).

On Mars, regolith grains are rounded due to long-term saltation by Martian winds, as directly observed by (Goetz et al. 2010) through optical microscope observations onboard the Phoenix spacecraft. Previous studies showed that the NE34 Fontainebleau sand could be a proper Martian regolith simulant (Delage et al. 2022). Fontainebleau sand is a well-sorted silica sand (grain density ρ_s = 2.651 Mg/m^3) from the Paris Basin with a D_{50} of 220 μm, compared with the D_{50}=175 μm diameter derived from thermal inertia measurements.

Previous investigations on Martial regolith allowed providing some first estimates of the compression and shear velocities of Mars's surface (Delage et al. 2017), together with other physical properties (Spohn et al. 2018), the interaction between the SEIS foot and the Martian regolith (Delage et al. 2022) and the study of the shear and compressive wave's velocity and Poisson ratio, among others.

Given that little information is available about the shear modulus degradation curve in sands below σ_3=30 kPa, a new specific device, using a DMA rheometer, was used to investigate very low stresses. This paper describes this new system and the tests carried out to investigate the degradation curve of the shear modulus at very low stresses and from low to large shear strains.

Background

Cyclic loading is a load repeatedly applied with a specific frequency (Ishihara 1996). Cyclic loading is of practical relevance for many problems in geotechnical engineering on Earth and other planets (e.g., Mars). It may be caused by human activities, like traffic, or natural sources, like seismic loads leading to the propagation of shear waves in the soil and inducing cyclic shearing (Wichtmann 2016). The dynamic shear modulus G and the damping ratio ξ characterized the soil response to cyclic and dynamic loadings. The soil response depends on the soil characteristics (e.g., relative density, grain size distribution), and conditions (e.g., confining pressure and strain level) (Kramer 1996).

Ishibashi and Zhang (1993) analyzed the dynamic properties of G and ξ of available soil set experimental data, including non-plastic sands to highly plastic clays, evaluating the effects of plasticity and confining pressure σ_3. The research concludes that the Plastic Index (PI) is the main factor controlling stiffness for plastic soils. In contrast, for cohesionless soils, like sands, the confining pressures significantly affect the soil stiffness (Molina-Gómez et al. 2020).

In terms of confining pressure, it influences the mechanical behavior of soil. The maximum shear modulus G_{max} for granular materials strongly depends on the confining pressure σ_3. This dependency is usually analyzed through the general form of equation (1) (Molina - Gómez et al. 2020):

$$G_{max} = C\left(\frac{\sigma_3}{P_a}\right)^n f(e) \quad (1)$$

where C is a material coefficient that captures the influence of the particle shape and bonding or cementation of the particles, P_a is the atmospheric pressure and n is a power exponent that reflects the sensitivity of the stiffness modulus to the confining pressure, and $f(e)$ is a void ratio function (Molina - Gómez et al. 2020).

The dependency between the maximum shear modulus and confining pressure σ_3 determines that the level of soil resistance decreases when the confining pressure is low. In consequence, the understanding of soil behavior at low stress is essential to geotechnical engineering problems related to shallow foundations, slope stability with a risk of surface failure, tunnels with shallow overburdens, geotechnical structures subjected to static or cyclic loading under low confining stress (Huang 2015), or the effect of seismic wave register by the SEIS (Delage et al. 2022).

Researchers have developed several laboratory and field tests throughout history to assess how confining pressure σ_3 and strain levels γ affect a soil's mechanical properties G and ξ, evaluating different strain ranges and minimum confining pressures.

Regarding the confining pressure effect on soil properties, test procedures have been developed to evaluate the effect of low confining pressures; however, the dynamic properties (G, ξ) have been measured at a minimum confining pressure of σ_3=20kPa. Delfosse-Ribay et al. (2004) evaluated both G and ξ in a resonant column test on a natural Fontainebleau sand (D_{50} =220 μm) and mixtures with various grouting materials (Delfosse-Ribay et al. 2004). They showed that, for all materials, the confining pressure improves the shear modulus, with, however, a negligible effect on the damping ratio. More recently, Kumar et al. (2013) investigated the dynamic properties (G, ξ) of sand and sandy soil with fines in a confining pressure range σ_3= [20:300] kPa. They point out that both G and ξ are significantly affected by the confining pressure, showing that an increase in the confining pressure increases G and decreases ξ, with a significant increase in cyclic strength under higher confining pressures (Kumar et al. 2013). Delage et al. (2017, 2022) investigated dry sand's dynamic properties (G, ξ) at confining pressures $\sigma_3 \geq 20$ kPa and relative densities $D_r \geq 0.3$. In this research, resonant column and triaxial tests were used to explore the influence of pre-vibration cycles at two relative densities (Dr= [0.3,0.6]) and two confining pressures (σ_3= [100,300] kPa). The results showed a slight decrease in shear modulus with increased loading cycles, with a significant drop in damping ratio. In addition, increased confining pressure decreases the sand's damping ratio and reduces the effect of the number of pre-vibration cycles. More recently, Molina-Gómez et al.(2020), presented a detailed characterization of two historically liquefiable sands from the greater Lisbon area using bender elements and resonant columns evaluating a confining pressure range of σ_3=[30-200] kPa. The results showed that the damping ratio increases with strain level in the range $\gamma > 10^{-5}$ in both sands. Furthermore, results showed that ξ decreases as σ_3 increases. Despite the existing research, few of them explore the very

low-stress range $\sigma_3 \leq 30$kPa.

Alternatively, the loading frequency repetition and the strain level significantly impact the soil's response to dynamic loads. The strain magnitude determines the soil phenomena and the mechanical characteristics (Ishihara 1996). Generally, soil deformations in a range of $\gamma < 10^{-5}$ are elastic and recoverable; the associated phenomenon could be the vibration and wave propagation through the soil layer. In contrast, in a range of $\gamma = [10^{-4}\text{-}10^{-2}]$, the soil behavior is elasto-plastic, producing irrecoverable deformation. In this condition, the development of cracks or differential settlements appears. Also, for strains $\gamma > 10^{-2}$, the soil could suffer slides, compaction, or liquefaction at higher strain levels (Ishihara 1996).

The strain level effect is evaluated in different ranges depending on the device and test characteristics (see table 1). Generally, Insitu measurements include vibration tests evaluating strain ranges of $\gamma = [10^{-5}\text{-}10^{-3}]$ and seismic wave method evaluating ranges of $\gamma = [10^{-6}\text{-}10^{-5}]$ (Ishihara 1996). Laboratory tests have a wide range of strain levels. The bender elements measure the elastic material zone. These tests could measure the strain range of $\gamma = [10^{-6}\text{-}10^{-5}]$ (Ishihara 1996, Rio 2006, Irfan et al. 2020). The elastic zone and part of the elasto-plastic zone of the shear modulus degradation curve could be measured by the resonant column, which provides information in the strain range of $\gamma = [2\times10^{-6}\text{:}6\times10^{-3}]$ (Ishihara 1996, Molina - Gómez et al. 2020). The elasto-plastic zone properties could be measured by repeated loading tests, like the dynamic triaxial test, which measures higher strain levels ($\gamma \geq 10^{-4}$) evaluating the shear dynamic modulus G degradation. Also, devices like the cyclic direct simple test, provide strain data between the resonant column and the triaxial test $\gamma = [10^{-4}\text{:}10^{-3}]$, measuring the maximum dynamic shear modulus G_{max} at the limit of the elastic range.

In order to measure the entire elastic and elastoplastic strain range, combined methods have been developed. For example, the University of Texas at Austin developed the fixed free Resonant Column/Torsional Shear (RCTS) studying the behavior of geomaterials at shear strain ranging from $\gamma = [10^{-5}\text{:}10^{-3}]$ (d'Onofrio et al. 1999). Based on the design criteria of the RCTS, d'Onofrio et al. (1999) developed THOR, a new torsional shear apparatus composed of a torsional cyclic shear device incorporating an electromagnetic loading system with a high-resolution measurement system allowing better precision measurements at strains levels below of $\gamma < 10^{-5}$ (d'Onofrio et al. 1999). However, finding a single instrument suitable for measuring strains within the entire allowable range $\gamma = [10^{-6}\text{:}10^{-2}]$ was not possible. Consequently, two different transducers had to be used. Hence, rotations were monitored by a pair of micro-proximity and approximators (d'Onofrio et al. 1999).

The combination of the existing devices allows the evaluation of soil's elastic and elasto-plastic behavior in a strain range of $\gamma = [10^{-6}\text{:}10^{-2}]$. However, a single curve could not be guaranteed in all cases due to differences in the loading setups, the sample preparation, and the deformation measurements (Villacreses et al. 2020). Therefore, using one single device over a wide strain range $\gamma = [10^{-6}\text{:}10^{-2}]$ appears useful and can be achieved with an oscillating rheometer, often used in other engineering fields (asphalt engineering or food processing).

The DMA dynamic shear rheometer (Dynamical Mechanical Analysis) measures a shear strain range of $\gamma = [10^{-6}:10^{-2}]$. It applies a harmonic oscillatory stress or strain signal with a controlled frequency and strain amplitude, measuring the material dynamic properties G and ξ (Villacreses et al. 2020). Table 1 shows a summary of the strain level ranges that some devices could measure based on the references analyzed (Ishihara.1996; d'Onofrio et al. 1999, Molina - Gómez et al. 2020, Rio 2006, Irfan et al. 2020, Villacreses et al. 2020). The rheometer test used in this research is a single device (not a combined method) that can measure a whole strain range from 10^{-6} to 10^{-2}.

TABLE 1. Shear strain ranges for soil dynamics tests measuring the shear modulus degradation

Test method	Strain Level
Rheometer	$10^{-6}:10^{-2}$
Bender Elements	$10^{-6}:10^{-5}$
Resonant Column	$2\times10^{-6}:6\times10^{-3}$
Repeated loading test (e.g., Cyclic Triaxial Test)	$10^{-4}:10^{-2}$
Combined Methods: Torsional shear+ Electromagnetic	$10^{-6}:10^{-2}$

Villacreses et al. (2020) tested kaolin samples in the DMA and subjected the samples to different suction conditions ψ= [0.35-98.5] MPa measuring a shear strain range of $\gamma = [6\times10^{-6}:1\times10^{-3}]$. The authors compared G and ξ with results obtained with the resonant-column apparatus, proving that the proposed method (DMA) could measure the soil behavior in a wider strain range and identify a G_{max} close to the value reported by the resonant column.

The results obtained by Villacreses et al. (2020) suggest that DMA had better precision than available tests for fine-grained soils. However, evaluating the dynamic soil properties of granular soils using DMA is challenging as dry granular soils require a confining pressure for holding the sample. Therefore, a careful preparation method is needed to ensure a uniform relative density across the sample.

The existing tests methods evaluate different strain ranges and confining pressures. However, a single device to evaluate the soil mechanical properties (G and ξ) for loose sands in a strain range of $\gamma = [10^{-6}–10^{-2}]$ and under low confinement pressures ($\sigma_3 < 10$ kPa) is currently missing. Also, the soil behavior under dynamic loads at low confining pressures requires further

investigation. Therefore, this study introduces a novel procedure using the DMA for loose dry sand, enabling the determination of dynamic parameters (G and ξ) across a wide strain range of $\gamma = [10^{-6}:10^{-2}]$ varying confining pressures $\sigma_3 = [3\text{-}30]$ kPa.

Experimental observations on cyclic degradation

To the author's knowledge, the first study points to soil modulus degradation measurements dating back to the mid-1930s with the resonant column works of Ishimoto (Ishimoto and Iida. 1936). However, the first documented observations relating shear strain with the shear modulus degradation in soils date back to the decade of the 1960s. In this decade, the dynamic characteristics were measured using standard devices, like the cyclic triaxial or the resonant column. First, the triaxial test measured the hysteresis loop of several coarse-grained soils (Weissman and Hart. 1962). Next, the effect of variables such as the void ratio and the degradation of the wave velocity was evaluated using the resonant column on sands (Hardin and Richart. 1963). Then, the observations of shear modulus degradation sparked the attention of the geotechnical community between 1966 and 1972, when the first degradation curves for the G moduli, on both sands and clays, were presented (Silver 1969, Seed 1970, Drnevich et al. 1966, Hardin and Drnevich 1972). Numerous works followed these early steps, relating the cyclic degradation in clays with the plasticity index. Similarly, for materials such as Toyoura sand, the presentation of the cyclic degradation in terms of normalized moduli G/G_{max} allowed a simpler comparison (Vucetic and Dobry 1991, Kokusho 1980).

The sample confining stress affects the degradation curves, showing a significant variation under slight variations in confinement. At stresses below σ_3=100 kPa, curves for different tests may be mixed, highlighting the relevance of test repeatability concerning the values' variability (Darendeli 2001).

Another key question lies in the interpretation of the degradation curve curvature. Semi-empirical fitting models that recreate the moduli degradation phenomena have addressed this question. These models are generally formulated regarding the normalized modulus as a function of the shear strain imposed upon the soil (Hardin and Drnevich 1972, Darendeli 2001).

Ishibashi and Zhang (1993) collected available data on dynamic shear moduli of various non-plastic sands and compared the data with a general equation for sandy soil relating the shear modulus with the confining pressure, expressed as equation (2).

$$\frac{G}{G_{max}} = K(\gamma)\,\sigma_3^{\,-m(\gamma)-m_o}$$

$$K(\gamma) = 0.5\left[1+\tanh\left\{\ln\left(\frac{0.000102}{\gamma}\right)^{0.492}\right\}\right]$$

$$m(\gamma)-m_0 = 0.272\left[1-\tanh\left\{\ln\left(\frac{0.000556}{\gamma}\right)^{0.4}\right\}\right] \qquad (2)$$

Ishibashi and Zhang (1993) also established an equation for the damping ratio related to G/G_{max}. However, the author mentioned that because measurements of damping ratio are more sensitive and challenging than the shear modulus measurements G and large damping ratios ξ would not be attained until the final stages of dynamic computations, the scatter of the data points was considered small, and it was fitted by equation (3) (Ishibashi and Zhang 1993).

$$\xi = 0.333\left\{0.586\left(\frac{G}{G_{max}}\right)^2 - 1.547\left(\frac{G}{G_{max}}\right) + 1\right\} \tag{3}$$

Besides the relation between the G_{max} and the confining pressure σ_3, the modified hyperbolic model is a general model that describes the shear modulus reduction of fine and granular soils. Santos and Gomes (2001), investigate the shear modulus degradation of soil with strain. The study was based on a key parameter defined previously by the authors and called reference threshold shear strain $\gamma_{0.7}$. This parameter was defined as the shear strain for a normalized soil stiffness degradation factor of G/G_{max}=0.7, in which G_{max} is the initial shear modulus for a very small strain ($\gamma=10^{-6}$), and G is the secant modulus of soil. The authors proposed a hyperbolic function used to fit test results. Simple regression analysis shows that the previous boundary curves can be fitted by a mean curve defined by the following relationship shown in equation (4). The best fitting was obtained with a=0.385 based on the least squares method.

$$\frac{G}{G_{max}} = \frac{1}{1 + a\left(\frac{\gamma}{\gamma_{0.7}}\right)} \tag{4}$$

More recently, Oztropak and Bolton (2016) calibrated the model's parameter to fit the results of 454 literature tests on granular soils. In addition, the model parameters were found based on a detailed review of an extensive experimental data collection for sands with various grain size distributions (Oztroprak and Bolton, 2016). Based on these calibrations, the model yields a relatively simple equation (5).

$$\frac{G}{G_{max}} = \frac{1}{\left[1 + \left(\frac{\gamma - \gamma_e}{\gamma_r}\right)^a\right]} \tag{5}$$

where the normalized soil stiffness G/G_{max} can be estimated as a function of the shear strain γ, a reference shear strain γ_r an elastic threshold strain γ_e, and a curvature coefficient α, varying between 0.75 to 1.0 (Oztroprak and Bolton. 2016).

According to the authors, the model may be used with G_{max} values directly measured from one of the experimental tests. Another option is to use it with the usual power models to predict the initial modulus value. The authors report that this model yields better predictions for higher strain values, and as is often the case, it has a significant uncertainty for low strains and stress values.

Materials and Methods

The DMA test is commonly used for determining the viscoelastic material properties of asphalt mixtures, like dynamic shear modulus and phase angle at different temperatures (Caro et al. 2013). The technique is also recommended for evaluating the deterioration of asphalt materials and their performance with temperature control (Caro et al. 2013). The test involves applying a harmonic oscillatory angular strain with frequency and amplitude control while measuring the necessary stress for maintaining the harmonic motion and the sample rotation with a precision of 10^{-9} N.m and 40 nrad, respectively (TA Instruments 2006). The measuring principle of the DMA is like the cyclic torsional test currently used to characterize cyclic soil behavior.

The DMA test directly and precisely measures the dynamic shear modulus G and damping ratio ξ. In this work, we adapt the DMA test by allowing basal suction σ_v and, hence, applying a confining pressure σ_3 to a dry sand sample (see fig. 2). In consequence, this procedure extends the experimental capabilities of the DMA to coarse-grained materials, allowing the study of the dynamic properties in a wider range of deformations and all in a single test.

This method's advantage is its ability to evaluate the dynamic soil response under a strain range $\gamma = [10^{-6}\text{-}10^{-2}]$ using a single device. Additionally, the rheometer provides precise values for each strain level with high accuracy. However, this procedure is specifically designed for dry sands with low confining pressures. To use this method on saturated sands, a system that blocks water from the vacuum system is required.

System device

Rheometers that apply cyclic signals of strains are known as Dynamical Mechanical Analysis (DMA) testers (Villacreses et al. 2020). The shear rheometer employed in this work has a minimum torque oscillation of 3×10^{-8} N.m and a minimum torque steady of 5×10^{-8} N.m. It could apply a minimum torque of 0.2 N.m, with a resolution of 1×10^{-9} N. Also, the motor has an inertia of 15 μ N.m.s and can apply an angular velocity in a range of 1×10^{-8} rad/s to 3×10^{-2} rad/s, with a displacement resolution of 4 x 10^{-5} rad (Villacreses et al. 2020, TA Instruments 2006).

In the shear rheometer, the sample is held on two metallic caps, tightened by two O-rings, and enclosed by a hand-made latex membrane. Initially, the piston directly contacts the sample, and the membrane is fitted onto the cap. Although the membrane may introduce additional confining stress, this effect can be disregarded when the vacuum is applied, as the membrane becomes stress-free. However, in larger deformations where the specimen is fully degraded,

the membrane remains embedded in the cap, resulting in recorded shear corresponding to the membrane. The confining pressure system is activated through a miniature hole on the bottom cap (see fig. 2). The DMA has a series of automated testing modes, among which the sweep shear strain is selected in this work.

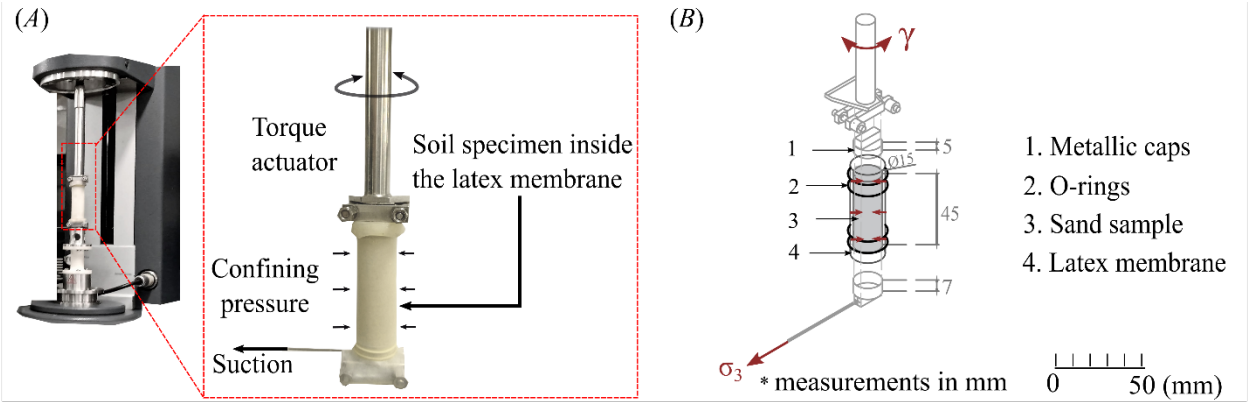

FIGURE 2. Schematic of the Dynamical Mechanical Analysis (DMA) for dry sands. (*A*) Experimental setup: photograph of the DMA Tester with a zoom of the sample; and (*B*) Sample dimensions, coupling system, and basal confinement.

The system device components have been designed especially for this test. First, the hand-made latex membrane is made using a rigorous proceeding with a smooth wood mold and submerged in liquid latex. The bottom and top caps are made of aluminum, matching the rheometer pedestal diameter. A rigid slice pipe of polyvinyl chloride supports the latex membrane while the sand sample is prepared. Table 2 shows the dimensions of the shear rheometer components.

TABLE 2. System device components dimensions and materials.

	Dimensions	**Material**
Bottom and Top Cap	Diameter: 15mm	Aluminum
Membrane	Diameter: 15mm Height: 60 mm Thickness: 2mm	Latex
Rigid slice pipe	Diameter: 15mm Height: 45 mm Thickness: 3 mm	Polyvinyl chloride
O-rings	Diameter: 15mm Thickness: 1 mm	Rubber

Material

Selecting a relevant Martian regolith simulant is challenging (Seiferlin et al. 2008). However, based on the measurements of the microscopic images of the Mars exploration rovers and Mars science laboratory, and Phoenix missions and by thermal inertia measurement, the Insight mission team has decided that t the Fontainebleau sand (NE34), well-sorted rounded sand with an average grain diameter D_{50}= 220 μm (close to 170 μm that is the estimated value at the InSight site) (Delage et al. 2022). Golombek et al. (2020) presented a geological description of the so-called 'homestead hollow' where the lander is located. Based on it, the Insight research team estimated the cross-section of the landing site with a layer around 3 m thick of relatively fine-grained impact-generated regolith that is likely to grade with depth into coarse, blocky ejecta, which overlies fractured basalt flows, with an estimated 10 m thick layer of blocky ejecta (Delage et al. 2022, Golombek et al. 2020).

Since one of the objectives in this research is evaluating the applicability of the DMA method on the Martian simulant regolith, experiments are performed on Fontainebleau sand, with a nearly monodisperse grain size distribution, mean grain diameter of D_{50} =220 μm, uniformity coefficient C_u = 1.52, void ratio range of [e_{min}: e_{max}] = [0.54: 0.84], and grain density of ρ_s=2.65 g/cm^3 (Delage et al. 2022). Figure 3 shows the grain size distribution obtained following the procedure of ASTM 6913 (ASTM 2017).

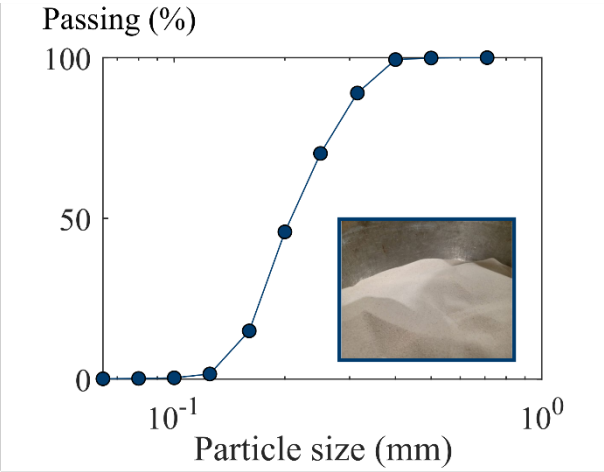

FIGURE 3. Grain distribution obtained of Fontainebleau Sand. Inset: Photograph of the sand sample.

Sample preparation

The sample preparation is the most critical and challenging step due to the sample's small dimensions and low density. The preparation process is carefully controlled, so replicability for all samples is guaranteed.

The DMA samples are prepared within a latex membrane and encapsulated within a rigid sliced pipe (see fig. 4*A*). The sliced pipe controls the sample dimensions, resulting in a sample of 15 mm in diameter. The space between the rheometer pedestal and the piston restricts the

sample height to 45 mm (see Table 2). The membrane is external to the system comprising the sample and the metallic caps. That is why when the rheometer piston goes down, it touches the sample directly.

Regarding the sample size, the proposed method applies only to fine sands. In fact, as noted in Gourves (1988, 1993) and Caicedo (2019), a relationship between the diameter of the sample and the maximum particle size sample $d_{sample}/ D_{max}>10$ is required to reach a coefficient lower than 10% in contact forces between particles. In this research, such a relationship is 375, ensuring that the sample behaves as a continuum.

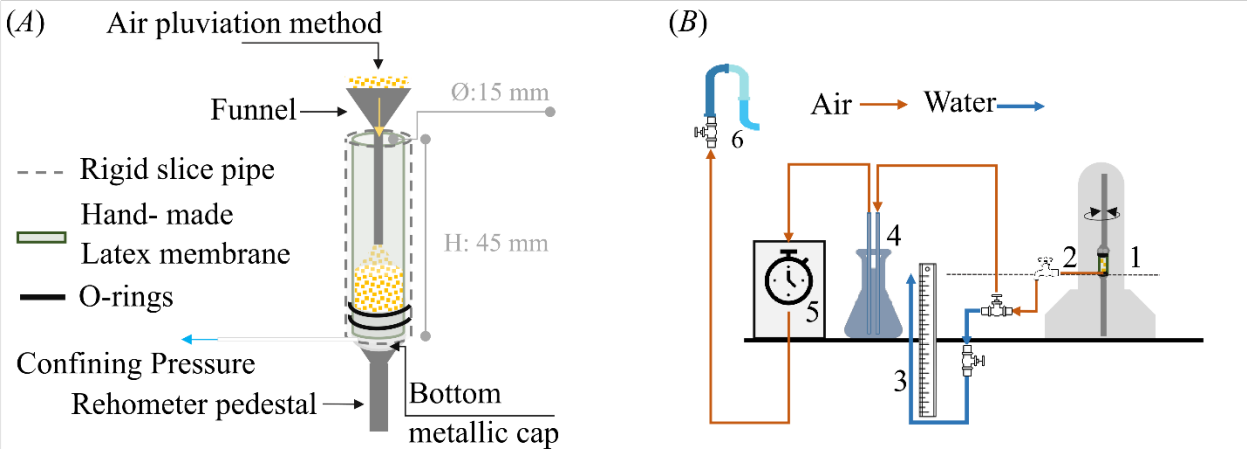

FIGURE 4. Schematics of the (*A*) Sample preparation and (*B*) water column method for a better precision measuring the confining pressure where: 1. Sample in the Rheometer's pedestal, 2. Suction through the cap hole, 3. Water column – ruler, 4. Water-sand trap, 5. Pressure gauge, and 6. Building's vacuum system.

The preparation procedure is as follows. First, the latex membrane is embedded in the bottom cap using two O-rings. Then, the rigid pipe covers the latex membrane giving support while the sample is prepared. Next, the sand is pluviated into the membrane using a funnel with a diameter of 5 mm. The funnel goes down until the bottom cap and the sand is deposited into the funnel. Then the funnel is raised, ensuring a release height close to zero. This process is essential in maintaining minimal external vibrations on the sample and avoiding possible densification. For control purposes, sample density is measured after the test, weighing the sand within the latex membrane, and obtaining variations of density of up to +/- 0.05 g/cm^3. Once the sample reaches the required density, the top rheometer motor is downed close to the sample. It is essential that the motor does not touch the sample and densifies it. Next, the latex membrane is tightened to the top and bottom DMA caps by two O-rings, ensuring a joined motion during the test (see fig. 4*B*). Once the sample height is reached and both caps are tight; air suction is applied through the bottom cap, inducing a confining pressure σ_3 on the sample.

Special care is devoted to inspecting for air leakages on the membrane fixtures or the membrane.

Low-confining pressures are controlled with a 100-mbar suction pump (reference: AGA VALVULA-EVAC 1000). For pressures below σ_3=10 kPa, we employed a water column method, guaranteeing a better precision measurement (see fig. 4*B*). In this process, the suction pump applies the confining pressure required through an air pipe joined to the bottom cap, but as the pressure is low, an additional method is necessary to regulate the measurement. First, the air pipe is bound to a water pipe using a water trap. Then, the water pipe allows the measurement of the water level, corresponding to the confining pressure applied. For pressures higher than σ_3= 10 kPa, the suction can be applied directly by the suction pump, obtaining better precision values with a precision of +/- 0.01 kPa.

Experimental campaign

The DMA tests are conducted on a Fontainebleau sand with a relative density of D_r= 0.2 +/- 0.05, subjected to a strain range of γ= [10^{-6}:10^{-2}] and maintain a constant shear strain rate frequency of f=1 Hz over ten harmonic signals. The frequency value was determined using a sweep frequency test to evaluate the frequency effect. Figure 5 shows the results of a frequency sweep test in a range of f= [0.01-8] Hz at a confining pressure of σ_3=5kPa and a constant strain level of γ=0.0004. This confining pressure was selected because it allows the evaluation of the effects of the frequency effects at very low confining pressure. Figure 5 shows that the frequency differs, showing a frequency effect. Due to this research following a shear strain sweep test, a constant frequency of f=1 Hz was selected as the constant value.

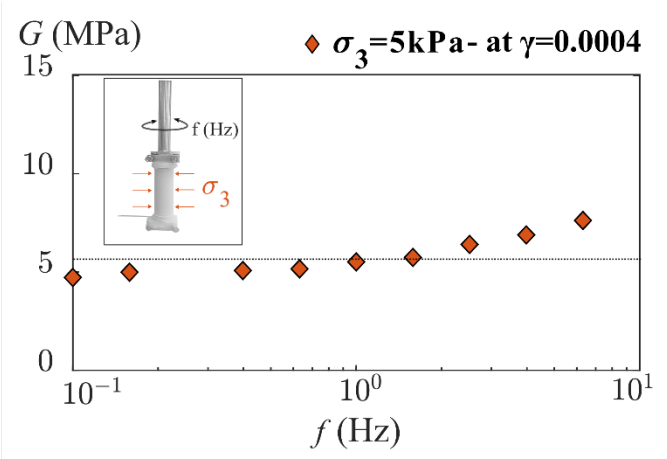

FIGURE 5. Frequency sweep test for a confining pressure of σ_3=5 kPa at a constant strain level of γ=0.0004.

The DMA test using the Rheometer is carried out using a strain sweep methodology that applies a sinusoidal torsional strain signal with a period of 1 min while the oscillation stress is recorded. This research tests the sand samples with a strain/displacement control. Each sweep

strain test consists of 13 strain levels in the range values of $\gamma = [10^{-6}:10^{-2}]$, applying ten harmonic sinusoidal signals with a period of 1 min (see fig.6). This procedure is adapted from the DMA test on kaolin samples by Villacreses et al. (2020).

The strain values increase during the test proportionally with piston rotation θ. Then, this rotation is converted into strain values according to the sample diameter and height. Besides the rotation, the DMA rheometer reports the values of the Torque (T) applied to the sample in values of (μN.m); these values are the basis of the shear stress calculation τ. Finally, the experimental variable is the confining pressure, while the strain range, density, and dimensions remain constant.

The adapted DMA allows testing the sand sample to very low confining pressures, like σ_3=3 kPa, until raising it to σ_3=30 kPa. For each confining pressure level, a total sweep shear strain is performed. Each confining pressure has three repetitions, confirming the test repeatability for DMA test. A sample is prepared for each confining pressure and test repeatability; once the swipe strain test ends, the system device is disassembled, cleaned, and assembled for the new test. Table 3 summarizes the experimental campaign. The harmonic signal is recorded for each strain level step. This is the base of the hysteretic loop, which is the basis for determining the dynamic properties *G* and ξ. Figure 6 shows how the hysteretic loop area increases as the strain level increases and how the hysteretic loop slope decreases.

TABLE 3. Experimental campaign.

	Dimensions	**Material**	**Condition**
Sample condition	Diameter: 15mm Height: 45 mm	Fontainebleau sand	Dry relative density: $\approx$ 0.2
	Swipe strain range	**Frequency**	**Confining pressure**
Test condition	$[10^{-6}:10^{-2}]$ Constant	1 Hz Constant	σ_3=[3 ,5,10,30]kPa

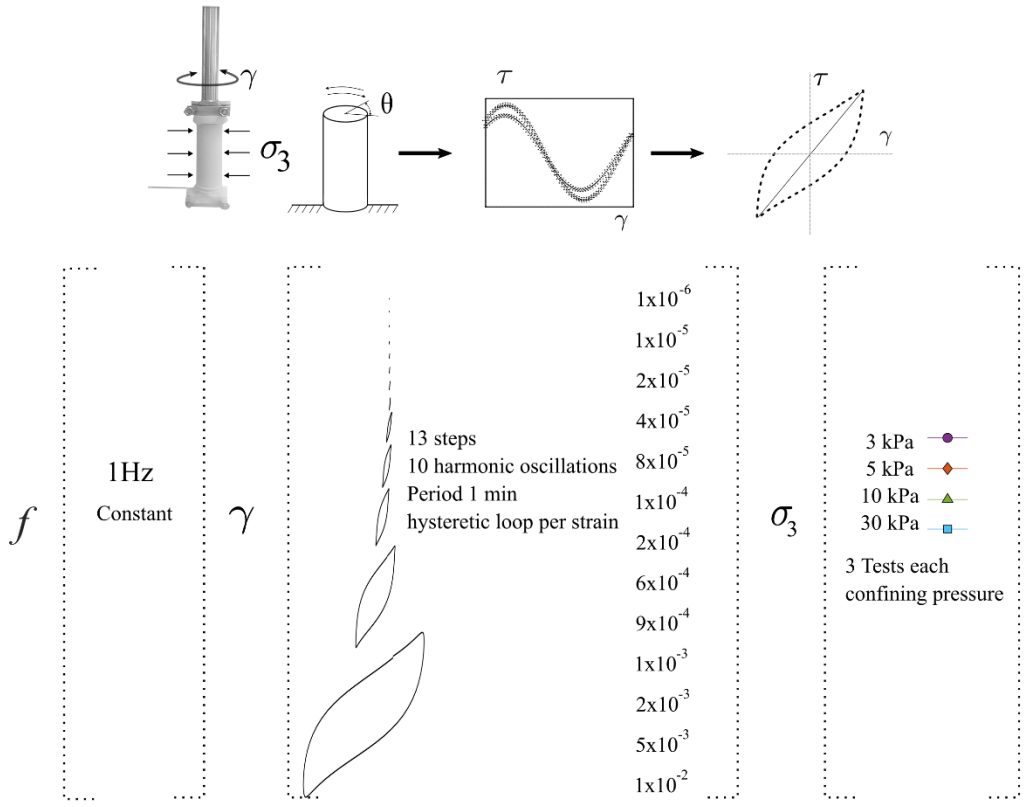

FIGURE 6. Scheme of the test campaign.

Results and Discussion

The sand's dynamic mechanical properties, G and ξ, can be evaluated using the harmonic signals recorded by the DMA rheometer. The recorded signals show a clean harmonic motion in time and allow the reconstruction of the hysteretic loop for each confining pressure (see fig. 7).

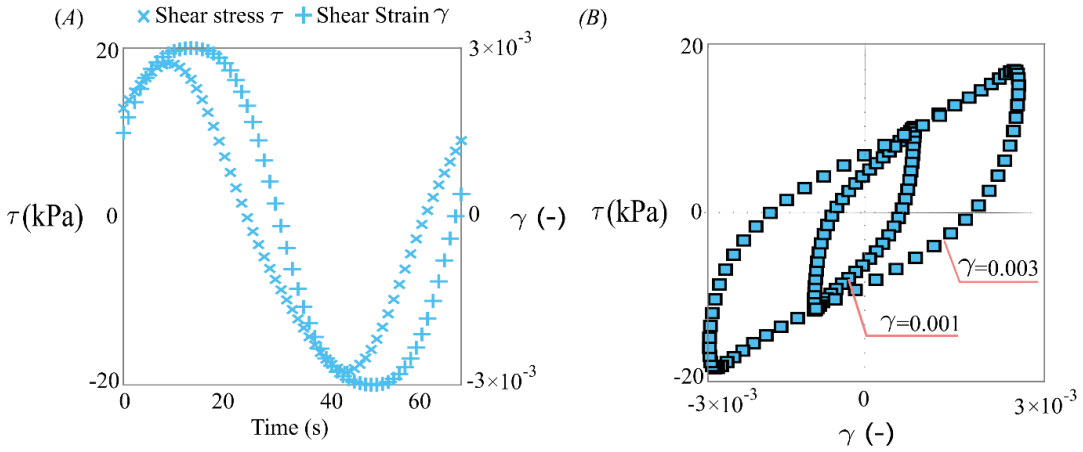

FIGURE 7. Example of a single oscillation recorded in the DMA test. (*A*) Torque and displacement harmonic and (*B*) Hysteretic loop indicating the dynamic shear module G measurement as the loop slope.

The hysteretic loops are recorded for each strain level, starting with the first strain level reported on the sample until the last strain level. Figure 8*A* shows the variation of the hysteretic loops for a confining pressure of σ_3=30kPa. The hysteretic loops size increase as the strain level increases. In contrast, the hysteresis loop slope decreases along the swipe strain test. Figure 8*B* shows the hysteretic loop for the first strain level recorded ($\gamma=5.2\times10^{-7}$). Comparing the first hysteretic loop with the lasted hysteretic loops ($\gamma\geq1\times10^{-3}$), the loop area is significantly higher for the last loop, showing a material energy dissipation during the test. The DMA test measured the properties of the first hysteretic loop, indicating that it can measure the sample's elastic range at the initial strain levels.

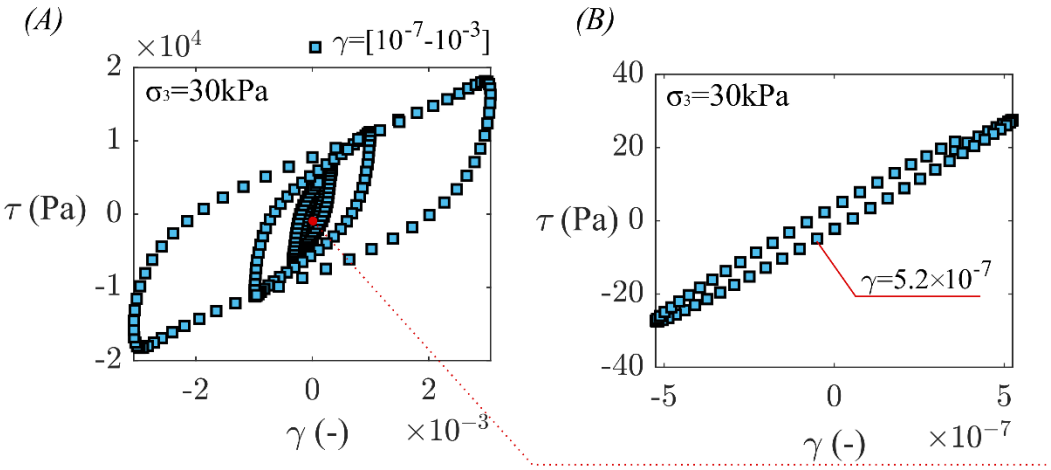

FIGURE 8. *(A)*Variation of the hysteretic loops for a confining pressure of σ_3=30kPa. *(B)* zoom in the first strain level.

Dynamic shear modulus

The hysteretic loop is the base of the dynamic measurements. Its slope depends on the soil stiffness *G* (see inset fig. 9*A*), which can be described by equation (6).

$$G=\frac{\tau}{\gamma} \tag{6}$$

Where τ is the shear stress related to the torque applied on the sample, and γ is the shear strain amplitude observed as the sample rotates (Kramer 1996).

The sweep strain test $\gamma=[10^{-6}\text{-}10^{-2}]$ is carried out for confining pressure $\sigma_3=[3,5,10,30]$ kPa with the three repetitions per confining pressure value. Figure 8 shows the mean value of the shear modulus obtained in each strain step and each confining pressure. Figure 8*A* shows the shear modulus evolution as the confining pressure increases, and Figure 8*B* shows the shear modulus degradation for each confining pressure. As shown in Figure 8*A*, the maximum shear modulus increases as the confining pressure increases. This stiffness increase is due to the increment in the hysteretic loop slope (see fig 9*A* inset). For example, for σ_3 =3 kPa, the

hysteresis loop has a slope close to zero because the material is loose, and the confining pressure is low.

In contrast, for σ_3 =30 kPa, the hysteresis loop inclination rises, pointing to a material stiffening and densification. The material is confined in this condition, and the elastic range extends to a strain level of $\gamma = 2\times10^{-5}$. The elastic range is evident for confining pressures of σ_3 =30 kPa and σ_3 =10 kPa; in these conditions, the material has more stiffness allowing a recoverable strain range. In contrast, as the confining pressures decrease, the material suffers a sudden degradation; hence, an elastic range is not evident for a confining pressure of σ_3 =3 kPa, and the *G* curve is almost linear. In contrast, an evident effect of low confining pressures is a relatively lower dynamic shear modulus *G* and normalized modulus G/G_{max} (see fig. 9*B*). However, the degradation rate increases as the confining pressure decreases, as σ_3 =30 kPa has the highest slope, followed by σ_3 =10kPa and σ_3 =5kPa. The degraded curve for σ_3 =3kPa does not present an evident elastic range and is suddenly degraded.

In all cases, the relationship between *G* and G/G_{max} with γ shows degradation at moderately large strains. Interestingly, this degradation is observed on very low γ for low confining pressures σ_3=3 kPa, while it only initiates at $\gamma \geq 2\times10^{-5}$ for σ_3=30 kPa. Here, it is assumed that the sand stiffness is minimal under low confinement, and the first oscillatory movement already degrades it. For this reason, the degradation curves for low confinement are linear, and an elastic range is not noticeable. Following the reasoning of an elasto-plastic material, the yield strain could set the transition between the elastic and the plastic ranges. This transition can be interpreted from the dynamic shear modulus degradation curve, and it can be argued that it depends on the confining pressure.

The results show that the degradation curve for 3 kPa points to a minimal elastic range from the test beginning and rapidly transitions to plastic behavior. On the other hand, the degradation curve of 30 kPa is more hyperbolic, or sigmoid, due to the transition from the elastic to the plastic range.

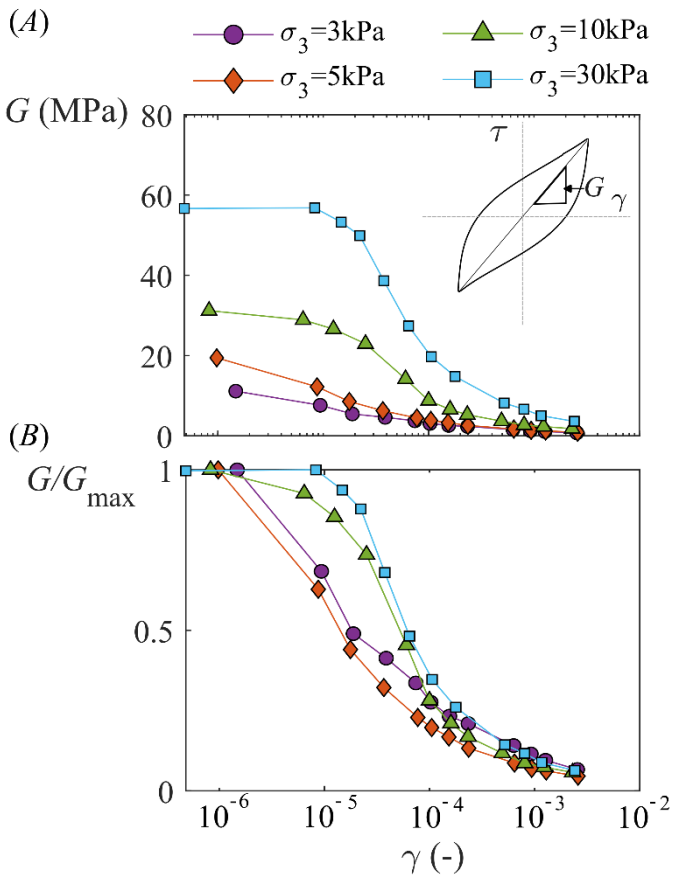

FIGURE 9. Shear modulus *G* degradation curve. (*A*) Evolution of *G* as a function of γ for confining pressures of σ_3= [3,5,10,30] kPa at *f*=1 Hz. Inset: Hysteretic loops for the same confining pressures at a shear strain level of γ=0.0010. (*B*) Normalized shear modulus G/G_{max} as a function of γ.

For a better precision degradation curve, it is helpful to compare the obtained results with the models proposed by Ishibashi and Zang, 1993 (equation (2)), Santos and Gomes Correia, 2001 (equation (3)), and Oztoprak and Bolton 2013 (equation (4)). Table 4 shows the nonlinear adjustment coefficient R^2. This coefficient of determination R^2 is a standard measure of goodness of fit for mathematical models fitted to empirical data using least squares regression (Kva° Lseth et al.1983). Kva° Lseth et al (1983) established that equation (7) is an appropriate measure of better precision for both linear and nonlinear models:

$$R^2 = 1 - \frac{\sum \left(G_{model} - \bar{G} \right)^2}{\sum \left(G_{model} - G \right)^2} \tag{7}$$

Where G_m are the fitted values obtained with the model, $\bar{G}$ is the mean value of the experimental results, and G the experimental shear modulus obtained with the DMA test. Following this statement, a good fitting is determined by the closeness of R^2 to 1.

TABLE 4. Coefficient of determination R^2 for the experimental degradation curves G/G_{max} at confining pressures σ_3=[3,5,10,30] kPa fitting with theoretical models.

σ_3	R^2		
Confining pressure Test (kPa)	Fitting with Ishibashi and Zang (1993)	Fitting with Santos and Gomes Correia (2001)	Fitting with Oztoprak and Bolton (2013)
3	0.6	0.7	0.6
5	0.8	0.8	0.6
10	0.8	0.9	0.9
30	0.9	0.9	0.8

The results show that Oztoprak and Bolton's (2013) model fit well with confining pressures higher than 10 kPa. In contrast, for lower confining pressure, the fitting decrease. Hence, the Oztoprak and Bolton model works better when a yield strain is evident, creating the need in future works to adapt the model for describing those materials under low confinement and with a minimal elastic range. However, Ishibashi and Zang (1993) and Santos and Gomes Correia (2001) still work for confining pressures $\sigma_3 \geq 5$kPa, as the adjustment coefficients are close to R^2=0.8. Figure 10 shows the degradation curves fitting with the theoretical models. The theoretical results validate the experimental results. For example, the Ishibashi and Zang (1993) equation model directly relates the G_{max} with the confining pressure, and this model presents the best fitting. Hence, these results demonstrate the capability of the DMA test to measure the dynamic shear modulus at low confining pressures.

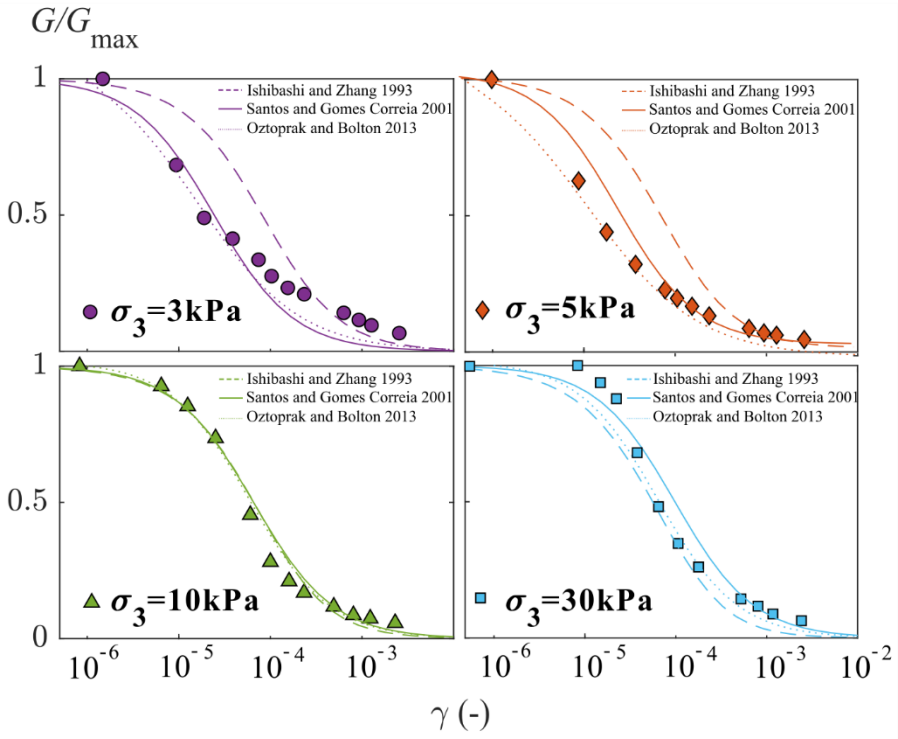

FIGURE 10. Degradation curves G/G_{max} at confining pressures σ_3= [3,5,10,30] kPa fitting with theoretical models.

Besides the model agreement, the DMA methodology shows repeatability in the results. Each confining pressure was repeated three times. To evaluate the repeatability capability of the DMA, a correlation coefficient is calculated for each confining pressure. The correlation coefficient is a quantity that gives the quality of the least squares fitting to the original data (Weisstein 2006). The correlation coefficient is used to determine the degree of association of variables. In multivariate experimentation (e.g., with three variables), it is often desirable to choose one's experiment. A convenient way of summarizing many correlation coefficients is to put them in a single table, called a correlation matrix. The correlation of any variable with itself is necessarily 1. Thus, the diagonals of the matrix are the unity, and as the correlation is close to 1, the data is similar, and the test device has high repeatability (Asuero et al. 2006). The DMA results for each confining pressure present high correlation values (higher than 0.9), showing the DMA's repeatability capability. Table 5 shows the correlation matrix for each test and confining pressure.

TABLE 5. The correlation coefficient for the three repetitions of the confining pressures σ_3= [3, 5,10, 30] kPa

3 kPa				5 kPa			
	Test 1	Test 2	Test 3		Test 1	Test 2	Test 3
Test 1	1.00			Test 1	1.00		
Test 2	0.97	1.00		Test 2	0.98	1.00	
Test 3	0.98	0.92	1.00	Test 3	1.00	0.99	1.00
10 kPa				30 kPa			
	Test 1	Test 2	Test 3		Test 1	Test 2	Test 3
Test 1	1.00			Test 1	1.00		
Test 2	1.00	1.00		Test 2	0.99	1.00	
Test 3	0.98	0.99	1.00	Test 3	0.97	0.98	1.00

Additionally, test series under confining pressures of σ_3= [3, 5, 10,30] kPa present standard deviation (σ) lower than σ =0.17 for the degradation curve lower. Also, the degradation shape is preserved, showing an elastic range at the beginning and a transition at $\gamma = 9\times10^{-5}$, then the dynamic shear modulus degrades (see fig. 11).

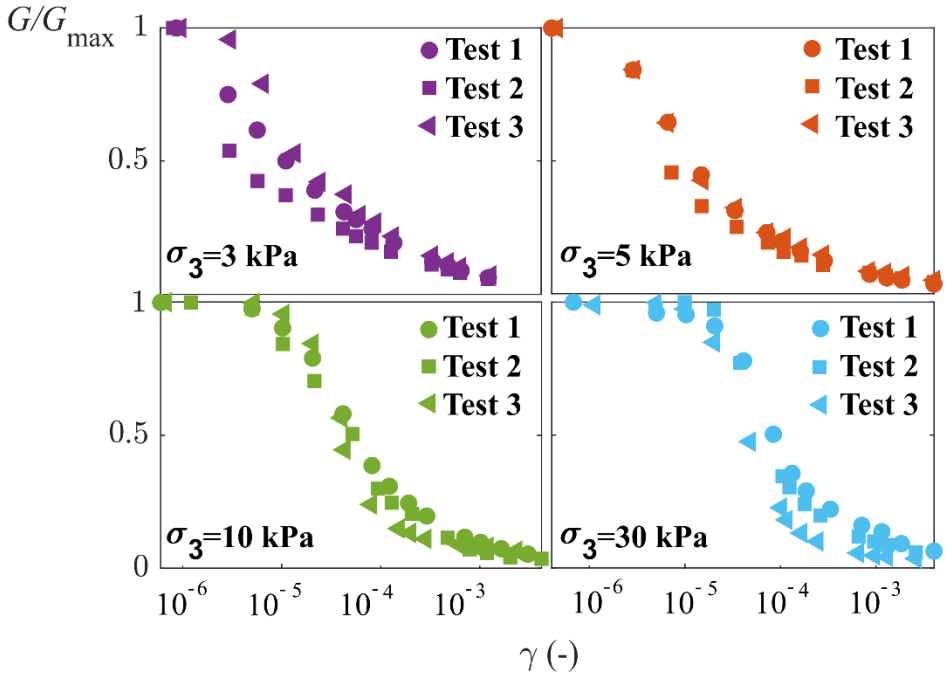

FIGURE 11. Test repetitions for shear modulus degradation curves for confining pressures of σ3= [3, 5,10, 30] kPa.

The reliability of the DMA results is measured with the reference results obtained by Molina_Gómez et al. (2020). In this research, a resonant column test was carried out on liquefied sand, on the TP-Lisboa sand with the same mean diameter as the Fontainebleau sand (D_{50}=0.22mm). The Resonant Column (RC) test was carried out in dry sand with a relative density of D_r=0.3 for confining pressures in a range of σ_3= [30-200] kPa (Molina_Gómez et al. 2020). Figure 12 shows the comparison between the DMA results and the RC results for a confining pressure of σ_3=30kPa obtained by (Molina_Gómez et al. 2020). The Fontainebleau has a higher degradation rate as it has less density than the TP-Lisboa sand. However, the results present standard deviations σ between the shearing strain levels lower than σ=15MPa in the shear modulus curve.

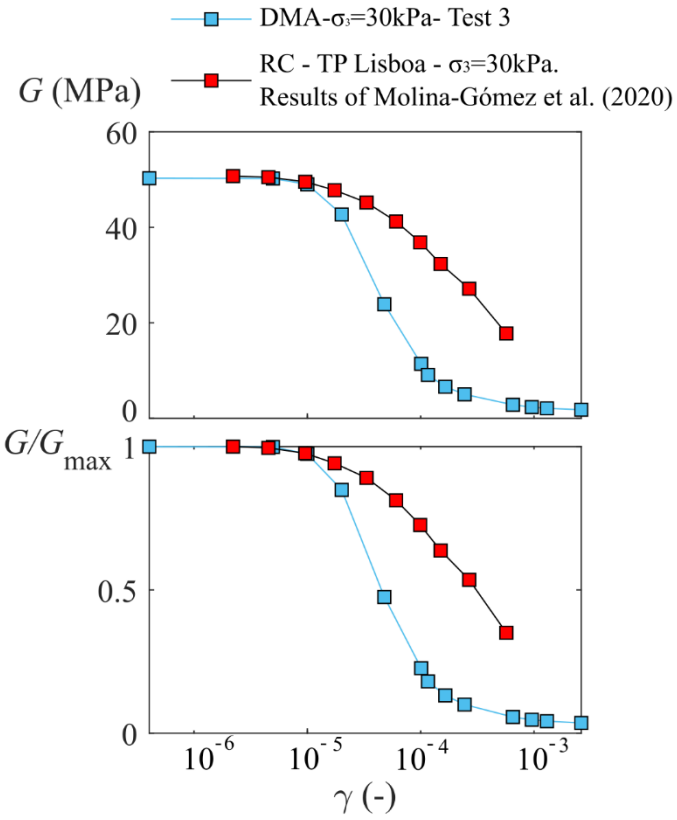

FIGURE 12. Comparison between Fontainebleau sand tested in the DMA in dry condition with a relative density of D_r=0.2, and dry TP Lisboa Sand results using Resonant Column (RC) with a relative density of D_r=0.2.

Damping ratio

The repeated shearing on the sand sample produces an energy loss that is related to an accumulation of plastic strains (Kramer 1996). An alternative for accounting for this energy dissipation is the hysteretic loop area (see the shaded area in fig. 13*B*). Both energy loss and dissipation are associated with the soil damping ratio ξ by the equation (8):

$$\xi = \frac{W_D}{4\pi\, W_s} = \frac{A_{loop}}{2\pi G\gamma^2} \tag{8}$$

where W_D is the dissipated energy, W_S is the maximum strain energy, and A_{loop} is the hysteretic loop area (Ishihara 1996 and Kramer 1996).

In a swipe strain test, at a constant confining pressure, the inner hysteretic loop area increases by increasing γ, representing a more significant energy dissipation as the sand is degraded (see fig. 13). As shown in Figure 13, the material under low confining pressures (σ_3=3 kPa) has a lower degradation of ξ comparing with higher confining pressures (σ_3=30 kPa). The curve for σ_3=3 kPa is less pronounced and falls between ξ =0.05 and ξ =0.11. However, the degradation is more significant for higher confining pressures (σ_3=30 kPa) and initiates for $\gamma>10^{-5}$. As shown in Figure 13, when the material is confined by σ_3=30 kPa, the damping ratio curve has an upward pick after a strain level of $\gamma=10^{-4}$. This behavior relates to the dynamic shear modulus degradation described in Figure 9. In contrast, for σ_3=3 kPa, the sand degradation can be assumed to occur under low-shear strains without showing a clear elastic range. Therefore, the damping ratio increment for σ_3=3 kPa is barely noticeable. Contrary, the damping ratio for σ_3=10 kPa and σ_3=30 kPa increases as the sand is degraded (see fig. 13). For σ_3=5 kPa, the elastic range is seen slightly, but after a strain level of $\gamma=10^{-5}$ behaves like σ_3=3 kPa.

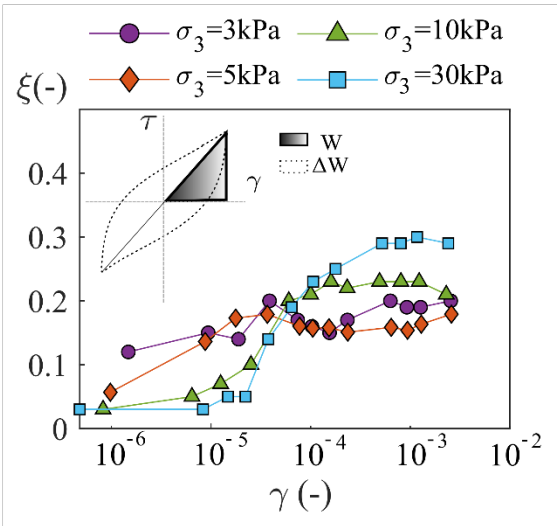

FIGURE 13. Damping ratio ξ at confining pressures of σ_3= [3, 5,10, 30] kPa at a cycle frequency of 1 Hz. Inset: Hysteretic loops showing a definition of the elastic stored energy and dissipation energy.

According to the theory for soil damping ratio (Delage et al. 2017, 2022), the results for σ_3 =10 kPa and σ_3 =30 kPa show an expected behavior, with the stiffness increasing as the confining pressure increases and the damping ratio presenting a symmetrical behavior with the shear strain. However, for σ_3 =3 kPa, results show that the damping ratio increases linearly

with strains, and the damping ratio is around 6% for low strains. This behavior constitutes a new finding of this study, which was observed thanks to the higher precision of the DMA under low confinements. The results show that using the DMA for sand allows the evaluation of the degradation curve in a wider strain range and the possibility to carry out tests at very low stress than the traditional methods.

The damping ratio results are compared with the model proposed by Ishibashi and Zang (1993) (equation (2)). Figure 14 shows the comparison between the theoretical model and the experimental results. For σ_3= [3,5,10,30] kPa, the coefficient of determination R^2 obtained corresponds to R^2 = [0.33,0.35,0.54,0.85], proving that the theoretical model fit with the experimental damping ratio for confining pressures higher than $\sigma_3 \geq 30$kPa, and highlight the limitations for a better precision fitting for lower confining pressures.

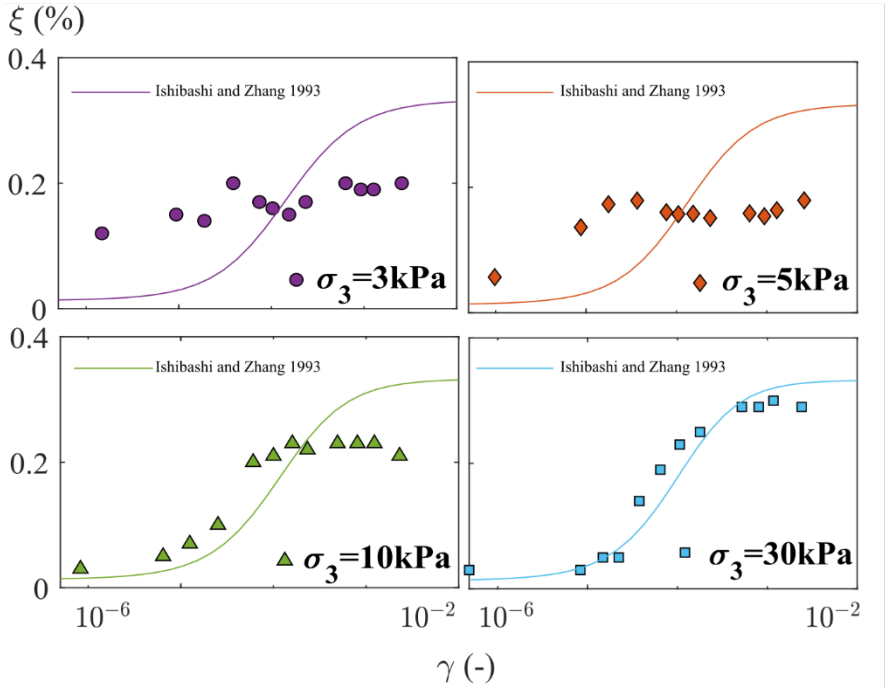

FIGURE 14. The damping ratio results σ_3= [3,5,10,30] kPa compared with the theorical model with a coefficient of determination R^2=[0.33,0.35,0.54,0.85

Conclusions

To better understand the dynamic parameters of the surface layer of regolith at the InSight landing site on Mars, an investigation of the dynamic properties of a regolith analog made up of sub-rounded loose Fontainebleau sand was carried out under stress and strain ranges significantly lower than in current practice in terrestrial soil mechanics. For his purpose, a Dynamical Mechanical Analysis (DMA) tester was used to evaluate the dynamic mechanical properties (shear dynamic modulus G and damping ratio ξ) of a sand loose sample ($D_r \approx 0.2$) submitted to confining pressures between σ_3=3 kPa to σ_3 =30 kPa at a frequency of 1 Hz. The experience shows that the DMA allows for high precision and good control of the shearing cycle. This characteristic allowed a better precision determination of the hysteretic loop. In

addition, using the rheometer in the geotechnical field proved simple and better precision, allowing for evaluating the dynamic properties of a loose sand sample at very low confining pressures in a wider strain range compared to traditional methods and all within a single soil test.

The results validated the new procedure, highlighting its ease of preparation, high precision, and versatile control of both frequency and amplitude. In addition, it was observed that the confining pressure controlled the shear modulus degradation, evidencing an elastic zone for a confining pressure of σ_3=30 kPa and a total degradation at lower confining pressures, like σ_3=3 kPa. Each confining pressure was tested at least three times, with similar values of the maximum dynamic modulus for each test and similar curve shapes.

The yield strain (an essential parameter of the shear degradation), clearly observed under high confining pressure, disappeared under low confinement. Further work is necessary to explore its link with the confining pressure in more detail. Also, the degradation rate and maximum shear modulus are related to the confining pressure. The material stiffness influences the soil damping. The damping ratio ξ increment for σ_3=3 kPa and σ_3=5 kPa is barely noticeable. Conversely, the damping ratio for σ_3=30 kPa and σ_3=10 kPa increases as the sand is degraded.

The theoretical models can capture the modulus degradation curve when the material is confined at σ3=30 kPa, as a yield strain is evident. However, for a confinement pressure of σ_3=3 kPa and σ_3=5 kPa, the models do not slightly miss the range under low strains and do not have the best fitting. This evidence the need for adapting the model to low confining pressures in further works. As a result, a comprehensive analytical framework could be elaborated for describing the degradation curves under a wider range of confinement pressures.

Finally, the new data obtained on the regolith analog must now be used in conjunction with the wave transfer at the surface of Mars to improve the analysis of the waves detected by the SEIS seismometer.

Acknowledgments

The authors would like to thank Eng. Jose Naranjo from Universidad de Los Andes for his ideas and technical support in the design and elaboration of the experiment. Also, the authors are grateful for the financial support provided by Universidad de Los Andes, Colombia.

References

ASTM International. 2017. *Standard Test Methods for Particle-Size Distribution (Gradation) of Soils Using Sieve Analysis*. ASTM D. 6913(2017). West Conshohocken. American Society for Testing and Materials, vol. 34. 2017. https://www.astm.org/d6913-04r09e01.html

Asuero, A. G., Sayago, A., and González, A. G. 2006. "The correlation coefficient: An overview". *Critical reviews in analytical chemistry*, No*36*(1): 41-59. https://doi.org/10.1080/10408340500526766

Caicedo, B. 2018." Geotechnics of roads: fundamentals". CRC Press.

Caro, S., Sánchez, D. B., and Caicedo, B. 2015. "Methodology to characterize non-standard asphalt materials using DMA testing: application to natural asphalt mixtures". *International Journal of Pavement Engineering* No16(1): 1-10. https://doi.org/10.1080/10298436.2014.893328

Darendeli, M. B. "A new family of normalized modulus reduction and material damping curves". Doctoral dissertation, University of Texas, 2001.

Delage, P., Betancourt, J. P. C., Caicedo Hormaza, B., Karakostas, F., De Laure, E., Lognonné, P., ... & Banerdt, B. 2022. "The interaction between the SEIS seismometer of the InSight Martian mission and a regolith simulant". *Géotechnique*: 1-12. https://doi.org/10.1680/jgeot.21.00171

Delage, P., Karakostas, F., Dhemaied, A., Belmokhtar, M., Lognonné, P., Golombek, M., De Laure, E., Hurst, K., Dupla, J. C., Kedar, S., Cui, Y. J. & Banerdt. 2017. "An investigation of the mechanical properties of some Martian regolith simulants with respect to the surface properties at the InSight mission landing site". *Space Science Reviews* No 211: 191-213. https://doi.org/10.1007/s11214-017-0339-7

Delfosse-Ribay, E., Djeran-Maigre, I., Cabrillac, R., and Gouvenot, D. 2004. "Shear modulus and damping ratio of grouted sand". *Soil Dynamics and Earthquake Engineering*, No 24(6): 461-471. https://doi.org/10.1016/j.soildyn.2004.02.004

Drnevich, V. P., Hall, J. R., and Richart, F. E. "Large amplitude vibration effects on the shear modulus of sand". Report to Waterways Experiment Station. Corps of Engineers. US Army Contact DA-22-079-Eng-340. University of Michigan,1966.

d'Onofrio, A., Silvestri, F., and Vinale, F. 1999. "A new torsional shear device". *Geotechnical Testing Journal* No 22(2): 107-117. https://www.astm.org/gtj11269j.html

GCTS. Dynamic hollow cylinder testing system (HCA-100). Retrieved from, https://www.gcts.com/pdf/products/Dynamic-Hollow-Cylinder-Test-Equipment. pdf

Goetz, W., Pike, W. T., Hviid, S. F., Madsen, M. B., Morris, R. V., Hecht, M. H., Staufer, U., Leer, K., Sykulska, H., Hemmig, E., Marshall, J., Morookian, J. M., Parrat, D., Vijendran, S., Bos, B. J., El Maarry, M. R., Keller, H. U., Kramm, R., Markiewicz, W. J., Drube, L., Blaney, D., Arvidson, R. E., Bell, J. F. III, Reynolds, R., Smith, P. H., Woida, P., Woida, R. & Tanner, R.. 2010. "Microscopy analysis of soils at the Phoenix landing site, Mars: Classification of

soil particles and description of their optical and magnetic properties". *Journal of Geophysical Research: Planets* No 115: E8. https://doi.org/10.1029/2009JE003437

Golombek, M., Warner, N. H., Grant, J. A., Hauber, E., Ansan, V., Weitz, C. M., Williams, N., Charalambous, C., Wilson, S. A., DeMott, A., Kopp, M., Lethcoe-Wilson, H., Berger, L., Hausmann, R., Marteau, E., Vrettos, C., Trussell, A., Folkner, W., Le Maistre, S., Mueller, N., Grott, M., Spohn, T., Piqueux, S., Millour, E., Forget, F., Daubar, I., Murdoch, N., Lognonné, P., Perrin, C., Rodriguez, S., Pike, W. T., Parker, T., Maki, J., Abarca, H., Deen, R., Hall, J., Andres, P., Ruoff, N., Calef, F., Smrekar, S., Baker, M. M., Banks, M., Spi. 2020. "Geology of the InSight landing site on Mars". *Nature Communications* 11 No. 1: 1–11. https://doi.org/10.1038/s41467-020-14679-1

Golombek, M. P., Haldemann, A. F. C., Simpson, R. A., Fergason, R. L., Putzig, N. E., Arvidson, R. E., Bell, J. F. III & Mellon, M. T. 2008. "Martian surface properties from joint analysis of orbital, Earth-based, and surface observations". In *The Martian surface-composition, mineralogy, and physical properties*, 468. Part of Cambridge Planetary Science.

Gourves. 1993. "Application of the Schneebli model in the study of micromechanics of granular media". *Mechanics of materials* No16 (1-2):125–131. https://doi.org/10.1016/0167-6636(93)90035-P

Gourves and F Mezghani.1988. "Micromécanique des milieux granulaires, approche expérimentale utilisant le modèle de schneebeli". *Revue Francaise de Geotechnique* N°4: 23-34. https://doi.org/10.1051/geotech/1988042023

Hardin, B. O., and Richart Jr, F. E. 1963. "Elastic wave velocities in granular soils". *Journal of the Soil Mechanics and Foundations Division*, No 89(1): 33-65. https://doi.org/10.1061/JSFEAQ.0000493

Hardin, B. O., and Drnevich, V. P. 1972. "Shear modulus and damping in soils: design equations and curves". *Journal of the Soil mechanics and Foundations Division*, No 98(7): 667-692. https://doi.org/10.1061/JSFEAQ.0001760.

Huang, Y, Cheng, H. L, Osada, T, Hosoya, A, and Zhang, F. 2015. "Mechanical behavior of clean sand at low confining pressure: Verification with element and model tests". *Journal of Geotechnical and Geoenvironmental Engineering* No 141: https://doi.org/10.1061/(ASCE)GT.1943-5606.000133

Irfan, M., Cascante, G., Basu, D., and Khan, Z. 2020. "Novel evaluation of bender element trans mitter response in transparent soil". *Geotechnique* No 70: 187–198. https://doi.org/10.1680/jgeot.17.P.256

Ishibashi I, Zhang X. 1993. "Unified dynamic shear moduli and damping ratios of sand and clay". *Soils Found* No 33:182-91. https://doi.org/10.3208/sandf1972.33.182

Ishihara, K.1996. *Soil Behaviour in Earthquake Geotechnics*, 1st ed. Oxford: Clarendon Press.

Ishimoto, M., and Iida, K. 1936. "Determination of Elastic Constants of Soils by means of Vibration Methods: Part I. Young's Modulus". *Bulletin of Earthquake Research Institute* No 14: 632-656.

Kva° Lseth, T. O. "Note on the R2 measure of goodness of fit for nonlinear models". *Bulletin of the Psychonomic Society*, *21*(1), 79-80, 1983.

Kramer, S. L. 1996. Geotechnical earthquake engineering. Pearson Education India.

Kokusho, T. 1980. "Cyclic triaxial test of dynamic soil properties for wide strain range". *Soils and foundations*, No 20(2): 45-60. https://doi.org/10.3208/sandf1972.20.2_45

Kumar, S. S., Krishna, A. M., and Dey, A. "Parameters influencing dynamic soil properties: a review treatise". Paper presented at the *National conference on recent advances in civil engineering,* pages1-10. 2013.

Molina-Gomez F., Viana da Fonseca A., Ferreira C., and Camacho-Tauta J. 2020. "Dynamic properties of two historically liquefiable sands in the Lisbon area". *Soil Dyn Earthq Eng* No 132: 106:101. https://doi.org/10.1016/j.soildyn.2020.106101

Oztoprak, S., and Bolton, M. D. 2013. "Stiffness of sands through a laboratory test database". *Géotechnique,* No 63(1): 54-70. https://doi.org/10.1680/geot.10.P.078

Rio, J.F. "Advances in laboratory geophysics using bender elements". Ph.D. Thesis University College of London, 2006.

Santos JA and Gomes Correia A. "Reference threshold shear strain of soil. Its application to obtain a unique strain-dependent shear modulus curve for soil". In: Proceedings of the 15th international conference on soil mechanics and geotechnical engineering. Istanbul, Turkey, 2001.

Seed, H. B. Soil moduli and damping factors for dynamic response analyses. Reoprt, EERC-70. In Report N° EERC 70-10 Earthquake Engineering Research Center (pp. 70-10). University of California, Berkley, 1970.

Seiferlin, K., Ehrenfreund, P., Garry, J., Gunderson, K., Hütter, E., Kargl, G., Maturilli, A. & Merrison, J. P. 2008. "Simulating Martian regolith in the laboratory". *Planet. Space Sci. 56* No. 15: 2009–2025. https://doi.org/10.1016/j.pss.2008.09.017

Silver, M. L., and Seed, H. B. "The behavior of sands under seismic loading conditions". Doctoral dissertation, University of California, Berkeley, 1969.

Spohn, T., Grott, M., Smrekar, S. E., Knollenberg, J., Hudson, T. L., Krause, C., ... and Banerdt, W. B. 2018. "The heat flow and physical properties package (HP 3) for the InSight mission". *Space Science Reviews* No 214:1-33. https://doi.org/10.1007/s11214-018-0531-4

TA Instruments, M. 2006. AR 2000 Rheometer. Rheometric Series Operator's Manual. TA Instruments, pp. 1-144.

Trebi-Ollennu, A., Kim, W., Ali, K., Khan, O., Sorice, C., Bailey, P., ... and Lin, J. 2018. "InSight Mars lander robotics instrument deployment system". *Space Science Reviews* No 214:1-18. https://doi.org/10.1007/s11214-018-0520-7

Villacreses, J. P., Caicedo, B., Caro, S., and Yépez, F. 2020. "A novel procedure to determine shear dynamic modulus and damping ratio for partial saturated compacted fine-grained soils". *Soil Dynamics and Earthquake Engineering* No 131: 106029. https://doi.org/10.1016/j.soildyn.2019.106029

Vucetic, M., and Dobry, R. 1991. "Effect of soil plasticity on cyclic response". *Journal of geotechnical engineering*, No 117(1): 89-107. https://doi.org/10.1061/(ASCE)0733-9410(1991)117:1(89)

Weissman, G. F., and Hart, R. R. "The damping capacity of some granular soils". In Proceedings of the Symposium on Soil Dynamics (pp. 45-54). West Conshohocken, Pennsylvania: ASTM International. January, 1962.

Weisstein, E. W. 2006. Correlation coefficient. *https://mathworld.wolfram.com*

Wichtmann, T. "Soil behaviour under cyclic loading-experimental observations, constitutive description and applications". Habilitation thesis. Karlsruhe Institute for Technology KIT, 2016.